Soft Matter

PAPER

View Article Online
View Journal | View Issue

Cite this: *Soft Matter*, 2014, **10**, 718

Bridging interactions of proteins with silica nanoparticles: The influence of pH, ionic strength and protein concentration†

Bhuvnesh Bharti,‡*[a] Jens Meissner,[a] Sabine H. L. Klapp[b] and Gerhard H. Findenegg*[a]

Received 11th September 2013
Accepted 5th November 2013

DOI: 10.1039/c3sm52401a

www.rsc.org/softmatter

Charge-driven bridging of nanoparticles by macromolecules represents a promising route for engineering functional structures, but the strong electrostatic interactions involved when using conventional polyelectrolytes impart irreversible complexation and ill-defined structures. Recently it was found that the electrostatic interaction of silica nanoparticles with small globular proteins leads to aggregate structures that can be controlled by pH. Here we study the combined influence of pH and electrolyte concentration on the bridging aggregation of silica nanoparticles with lysozyme in dilute aqueous dispersions. We find that protein binding to the silica particles is determined by pH irrespective of the ionic strength. The hetero-aggregate structures formed by the silica particles with the protein were studied by small-angle X-ray scattering (SAXS) and the structure factor data were analyzed on the basis of a short-range square-well attractive pair potential (close to the sticky-hard-sphere limit). It is found that the electrolyte concentration has a strong influence on the stickiness near pH 5, where the weakly charged silica particles are bridged by the strongly charged protein. An even stronger influence of the electrolyte is found in the vicinity of the isoelectric point of the protein (pI = 10.7) and is attributed to shielding of the repulsion between the highly charged silica particles and hydrophobic interactions between the bridging protein molecules.

1. Introduction

The interaction of proteins with nanoscale materials plays a key role in modern biotechnology and in the biomedical field.[1–3] Much research has therefore been devoted to better understand the fundamentals of protein adsorption.[4–11] It is well-established that proteins adsorb strongly onto hydrophobic surfaces, even under electrostatically adverse conditions, because the driving force for adsorption originating from dehydration of a hydrophobic surface largely outweighs electrostatic repulsion.[12,13] Protein adsorption onto hydrophilic surfaces depends on the conformational stability of the protein, and a distinction between structurally inflexible ("hard") and pliable ("soft") proteins has been introduced to account for differences in the adsorption behavior.[13] Whereas soft proteins can relax to a less ordered (higher entropy) state at the surface, hard proteins retain their native (low-entropy) structure. Their behaviour at hydrophilic/charged surfaces is dominated by electrostatic interactions, *i.e.*, adsorption will occur when the protein and surface are oppositely charged, but not otherwise.[13]

Protein adsorption on nanoparticles can be affected by the high surface curvature of the particles.[14–17] Much attention was paid to the question to what extent the structure of proteins is perturbed by adsorption onto hydrophilic or hydrophobic nanoparticles,[17–19] or if the interaction with their strongly curved surface can promote aggregation and fibrillation of proteins.[20,21] On the other hand, it is also possible that the adsorption of the protein causes bridging of two or more nanoparticles. Only a few studies so far have addressed protein-induced bridging aggregation of nanoparticles,[22–24] although the potentially bioadverse consequences of such particle aggregation effects are well recognized.[25]

We have studied the interaction of lysozyme, a small globular protein (dimensions about 3 × 3 × 4.5 nm),[26] with silica nanoparticles (20 nm) as a function of pH in dilute aqueous dispersions.[23] Lysozyme is a prototypical hard protein (its tertiary structure is stabilized by 4 internal disulfide bridges) with a high isoelectric point (pI = 10.7). Hence over a wide pH range the protein and silica particles (pI = 3) carry opposite net charges. Accordingly, the adsorption of lysozyme on the silica particles was found to be strongly pH dependent. No adsorption

[a]*Institut für Chemie, Stranski Laboratorium, TC 7, Technische Universität Berlin, Strasse des 17. Juni 124, D-10623 Berlin, Germany. E-mail: bhuvneshbharti@gmail.com; findenegg@chem.tu-berlin.de*

[b]*Institut für Theoretische Physik, PN 7-1, Technische Universität Berlin, Hardenbergstrasse 36, D-10623 Berlin, Germany*

† Electronic supplementary information (ESI) available: Characterization of silica nanoparticle dispersion, sedimentation seperation rates of the silica–lysozyme aggregates and images of silica–lysozyme hetero-aggregates at different pH values and salinities. See DOI: 10.1039/c3sm52401a

‡ Present address: Department of Chemical and Biomolecular Engineering, North Carolina State University, Raleigh, NC 27695, USA.

was found up to pH 4, as to be expected for hard proteins on uncharged hydrophilic surfaces. At higher pH, strong binding of the protein to a gradually increasing number of adsorption sites was observed, achieving dense monolayer coverage at pH 8.3, and even higher adsorption levels beyond this pH. In the entire pH regime between the isoelectric points of silica and lysozyme, protein-induced hetero-flocculation was observed, but the flocs re-dispersed at higher and lower pH. This reversible flocculation contrasts with the familiar situation of polymer-induced bridging flocculation.[27] Characterization of the aggregates by small-angle X-ray scattering (SAXS) displayed characteristic features of silica particles interacting by an effective short-range attractive potential, clearly distinct from the effective repulsive potential between silica particles in the absence of the protein.[28,29] The results of our study[23] were consistent with the notion that the negatively charged silica particles are bridged by the oppositely charged and relatively rigid protein molecules.

Here we study the influence of ionic strength on the pH dependent bridging aggregation. The addition of an electrolyte will suppress the strength and range of the repulsive interaction between the positively charged protein molecules and between the negatively charged silica particles, but also it will screen the attractive interaction between protein molecules and the silica particles. For 1 : 1 electrolytes the screening length (Debye length) decreases from *ca.* 10 nm to 1 nm when the ionic strength is increased from 1 mM to 100 mM.[29] The layer of the adsorbed protein has a thickness of a few nanometers. Hence in a 1 mM salt solution the electric double layer extends beyond the layer of the adsorbed protein, but at 100 mM salt the protein layer shields the surface–protein contact region from the solution. This implies that the surface charge will be largely compensated by counterion adsorption onto the contact region.[12] In the present context we are interested in the consequences of this salt-induced charge neutralization effect on the protein-induced aggregation of silica particles. Since protein molecules act as bridges between the silica particles, the number ratio of protein molecules and silica particles may also be an important determinant for the structure of the hetero-aggregates. This conjecture was tested by studying the effective interaction between the bridged silica particles as a function of electrolyte concentration and for different protein-to-silica particle number ratios.

2. Theoretical background

2.1 SAXS from silica–protein dispersions

Scattering of X-rays from colloidal dispersions results from the difference in the mean electron density between the particles and the surrounding medium. In the present system we have two types of particles, *viz.* silica nanospheres and lysozyme molecules, but scattering arises mostly from the silica nanospheres, as a result of their larger size and higher X-ray scattering contrast against the aqueous medium compared to the protein (see Appendix). To a good approximation, the SAXS data can therefore be analyzed by the formalism for single-particle dispersions. The effects caused by the protein are seen indirectly *via* their influence on the interaction and structural correlation among the silica particles. The scattered intensity $I(q)$ as a function of the magnitude of the momentum transfer q is then given by

$$I(q) = \Delta\rho^2 \varphi_p V_p P(q) S(q) \quad (1)$$

where $\Delta\rho$ is the electron density contrast, φ_p is the volume fraction of the particles in the system, V_p is the volume of a single particle, $P(q)$ is the form factor of a particle, and $S(q)$ is the structure factor which accounts for the correlations between the particles in the dispersion. It will be demonstrated that protein adsorption has only a marginal influence on the particle form factor. For the dilute silica dispersions studied in this work ($\varphi_p \approx 0.0045$) the interactions between the particles are negligible in the absence of the protein. Accordingly, the structure factor of the silica–protein composite systems can be derived experimentally by dividing $I(q)$ of the dispersion by the form factor of the silica nanospheres obtained by fitting $I(q)$ of a silica dispersion without protein ($y = 0$),[28]

$$S(q) = \frac{\left[I(q)/\varphi_p\right]_{y>0}}{\left[\Delta\rho^2 V_p P(q)\right]_{y=0}} \quad (2)$$

2.2 Colloidal fluid model

Bridging of two silica particles by the adsorbed protein corresponds to a short-range attractive interaction between the two silica particles. A simple model describing this effective interaction is the square-well (SW) potential[30]

$$V_{SW}(r) = \begin{cases} +\infty & r < \sigma \\ -\varepsilon & \sigma < r < \sigma + \Delta \\ 0 & r > \sigma + \Delta \end{cases} \quad (3)$$

which accounts for excluded volume effects associated with the hard-core diameter σ plus an attractive well of width Δ and strength ε. The state of the system depends on the packing fraction $\varphi = (\pi/6)n\sigma^3$ (where n denotes the number density of particles) and a reduced temperature $T^* = k_B T/\varepsilon$ (where k_B is the Boltzmann constant and T is the experimental temperature). For given values of φ and T^*, only the well width Δ remains a free parameter. This degree of freedom disappears in the sticky-hard-sphere (SHS) limit,[31] where one takes the combined limits $\varepsilon \to \infty$ (*i.e.*, $T^* \to 0$) and $\Delta \to 0$, while keeping constant the so-called stickiness parameter $\tau^{-1} \equiv [12\Delta/(\sigma + \Delta)]e^{\varepsilon/k_B T}$. The dimensionless parameter τ is proportional to the temperature, while τ^{-1} is a measure of stickiness of the particles. The case $\tau^{-1} = 0$ corresponds to nonsticky hard spheres. The structure factor of a fluid of particles interacting by a sticky-hard-sphere potential can be calculated analytically from the (exact) Ornstein–Zernike equation combined with the Percus–Yevick (PY) approximation.[32] The results are in good agreement with Monte Carlo simulations of the SHS fluid.[33] For the square-well fluid there is no analytical solution of the integral equations (in any closure approximation), but analytical results may be obtained by considering the attractive well as a perturbation of the hard-sphere potential.[34] To compare the structure factor of the SHS fluid with that of the SWPY fluid, one has to define an effective

temperature $\tau_e(T^*, \Delta)$. Commonly the criterion imposed is that the second virial coefficient of the SW fluid be equal to that of the SHS fluid, *i.e.*, $B_2^{SW}(T^*, \Delta) = B_2^{SHS}(\tau_e(T^*, \Delta))$. This yields[33]

$$\tau_e(T^*, \Delta) = [4(\lambda^3 - 1)(e^{\varepsilon/k_BT} - 1)]^{-1} \quad (4)$$

with $\lambda = 1 + \Delta/\sigma$. Alternative criteria for the equivalence of the two models have also been suggested.[30,35] It was shown[33] that the analytical solution for the structure factor of the SHS fluid and numerical solutions for the SW fluid are in good agreement over a wide range of volume fractions if the well width is small against the particle diameter ($\Delta/\sigma < 0.1$). In this case some ambiguity of the SW model, arising from the fact that different combinations of the parameters Δ and ε yield nearly the same structure factor, can be avoided by mapping the SW model into the SHS model with an effective stickiness τ_e^{-1} given by eqn (4). In the present work the structure factor data were fitted with the parameters Δ, ε and φ; subsequently, τ_e was calculated with eqn (4).

3. Materials and methods

3.1 Materials and sample preparation

Two samples of silica nanoparticles (SNP1 and SNP2) were synthesized and purified as in our preceding work,[23] using the basic amino acid lysine instead of ammonia as a catalyst for the hydrolysis of tetraethyl orthosilicate (TEOS).[36] The nanoparticles were characterized by SAXS, nitrogen adsorption, and TEM (Fig. S1, ESI†). The mean diameter D and polydispersity δ of the particles were obtained by fitting the SAXS data with the polydisperse spherical bead model with log-normal size distribution. The specific surface area of the samples was determined by the BET method and compared with the corresponding geometric area, $a_{geo} = 6/D\rho$, with $\rho = 2.2$ g cm^{-3} the mass density of silica. The number of silica particles per mL of the dispersion, N_{NP}, was calculated from the mass concentration, the particle diameter D and silica density ρ. The characterization parameters of the two silica dispersions used in this study are summarized in Table 1. Lysozyme from hen egg white (Sigma-Aldrich, lot no. 019k1320, molecular weight 14.3 kDa) was used in this study without further purification. Previous X-ray scattering studies on lysozyme dispersions at pH 4.5 have reported a radius of gyration of 1.5 nm for the protein.[37]

Samples investigated in this study were prepared by adding a 1.1 mg mL^{-1} unbuffered lysozyme solution to a silica dispersion at neutral pH, and an appropriate amount of dry NaCl was added. The pH of the dispersion was then adjusted by adding small aliquots of 1 M HCl or NaOH, until the pH remained constant within 0.1 pH units. Since the protein adsorption is causing an initial pH change, the final pH of the dispersion was measured after 24 hours of equilibration at room temperature.

Table 1 Characteristics of the LysSil silica nanoparticles

Silica sample		SNP 1	SNP 2
Mean particle diameter	D/nm	18.7	21.7
Polydispersity	Δ	0.13	0.10
Specific surface area	a_{BET}/m^2 g^{-1}	188	172
Surface area ratio	a_{BET}/a_{geo}	1.29	1.37

3.2 Methods

SAXS. Measurements were performed on a SAXSess mc^2 instrument (Anton Paar, Austria), which was equipped with a Cu Kα slit-collimated radiation source operated at 40 kV (50 mA). The sample-to-detector distance was 309 mm. The scattered intensity $I(q)$ is obtained as the function of scattering vector $q = (4\pi/\lambda)\sin\theta$, where $\lambda = 0.1542$ nm and 2θ is the scattering angle. A fluid flow cell with 1 mm quartz capillary was used. Each data point $I(q)$ represents the average of the scattering output intensity of 500 measured frames. The Saxsquant 3.50 software was used for data reduction. The datasets were normalized by using the primary beam intensity as a standard. The dark current and water background were subtracted and the desmearing process was performed using the corresponding beam length and width profiles. The SASfit software[38] was used for further data analysis.

Analytical centrifuge. The dispersions were also characterized by sedimentation studies using a LUMiSizer analytical photocentrifuge (LUM, Germany).[39,40] Sedimentation profiles were determined at a centrifugal acceleration of 36g (bottom position). Subsequently, the compression kinetics of the sediment was determined at 2300g. The size distribution of flocs was determined in separate measurements in which the centrifugal acceleration was gradually increased from 13g to 2300g.

4. Results

The influence of pH and added electrolyte on the adsorption of lysozyme and the concomitant protein-induced aggregation of silica particles was studied at a fixed silica concentration (1 wt%) and different amounts of protein. The samples are specified by the number of protein molecules per silica particle, $y = N_{Lyz}/N_{NP}$. Characteristics of the studied samples are given in Table 2.

4.1 Protein binding and hetero-aggregation

Fig. 1 shows the protein binding and hetero-aggregation characteristics of sample A ($y = 38$) as a function of pH in the absence of salt and for two salt concentrations (10 and 100 mM NaCl). In Fig. 1a, protein binding is expressed by the mass of adsorbed lysozyme per unit surface area of silica, and by the fraction of the bound protein f. In all cases protein binding starts somewhat above pH 4 and reaches a level of 0.65 ± 0.02 mg m^{-2} at pH > 7, consistent with complete binding of 1.2 mg lysozyme to 0.01 g of SNP1 (0.64 mg m^{-2}, with the specific surface area from Table 1). Accordingly, all protein is bound at pH > 7 (complete-binding regime). Fig. 1a shows that the protein binding curves for the three different ionic strengths coincide within experimental error over almost the entire studied pH range. This finding was confirmed in repeated experiments. A distinct salt effect was observed only at the highest experimental pH value (pH = 10.5), at which incomplete binding of lysozyme was found at the highest salt concentration.

Table 2 Characteristics of silica–protein samples

Dispersion		Sample A $y = 38$	Sample B $y = 11$
Silica volume fraction[a]	φ	0.0045	0.0045
No. of particles per mL	N_{NP}/mL^{-1}	1.32×10^{15}	0.85×10^{15}
Mean particle separation	d/nm	91	106
Lyz molecules per mL	N_{Lyz}/mL^{-1}	5.05×10^{16}	0.99×10^{16}
Lyz surface concentration	Γ_0/nm^{-2}	26.9×10^{-3}	5.8×10^{-3}

[a] Based on the silica mass density $\rho = 2.2$ g cm^{-3}.

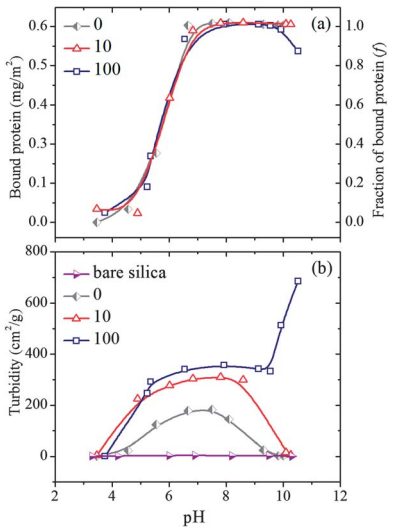

Fig. 1 Lysozyme interaction with silica nanoparticles in system A ($y = 38$) as a function of pH: (a) adsorbed amount of protein as a function of pH in the absence of added salt and for 10 mM and 100 mM NaCl; (b) turbidity of the dispersion as a function of pH for bare silica (triangles right) and for the added lysozyme with 0 (diamonds), 10 (triangles up) and 100 mM NaCl (squares).

The turbidity of the samples as a function of pH at different ionic strengths is shown in Fig. 1b in comparison with the low turbidity of the silica sample without protein. In the absence of lysozyme no silica aggregation was observed up to 100 mM NaCl in the studied pH range (not shown). For the protein-containing samples the turbidity starts to increase above pH 4, in parallel with protein binding (Fig. 1a). At low salt concentration (10 mM) the turbidity passes a maximum and returns to low values at pH 10. This behaviour is a signature of protein–silica hetero-aggregation and re-dispersion near the isoelectric point of the protein. At low electrolyte concentrations hetero-aggregation is completely reversible in pH, as it was found in the absence of the electrolyte.[23] At higher ionic strength (100 mM), however, a different aggregation behaviour is observed in the high pH regime, where the turbidity is not decreasing but sharply increasing with pH (Fig. 1b). The influence of ionic strength on the hetero-aggregation behaviour near pH 10 was studied in more detail by sedimentation measurements (see below).

The results presented in Fig. 1 are constitutive for the phenomenon of protein–silica hetero-aggregation induced by protein binding. An unexpected aspect revealed by the two graphs is that the diversity in the aggregation behaviour is not reflected in the protein binding characteristics. We return to this point in the Discussion section.

4.2 Aggregation properties from the sedimentation study

Analytical centrifugation was used to characterize the influence of ionic strength on the size and packing density of the silica–lysozyme hetero-aggregates at high pH. The distribution of aggregate size was determined from the time evolution of the transmission at a fixed sample height, as explained elsewhere.[39,40] Fig. 2a presents the cumulative volume-weighted size distributions for sample A ($y = 38$) at pH $\approx$ 11 at four salt concentrations from 10 to 100 mM. The resulting mean aggregate size L and size distribution ΔL as a function of the concentration of the added electrolyte are given in Table 3. It can be seen that at this high pH an increase in salt concentration causes a strong increase of the mean aggregate size. This finding is in line with the observed increase in turbidity with increasing electrolyte concentration at the highest pH (Fig. 1b).

The sedimentation rate of the silica–lysozyme dispersions was measured to determine the sediment volume as a function of centrifugal stress. Sediment volumes V_{sed} were determined by monitoring the boundary between the sediment and the supernatant (defined as the locus of 75% limiting transmission value) as a function of time at centrifugal accelerations of 36g and 2300g (Fig. S2 in the ESI†). The packing density (volume fraction) of silica particles in the aggregates was estimated from V_{sed} as $\varphi_s = m_s/(\rho_s V_{sed})$, where m_s is the total mass of silica in the sample and ρ_s is the mass density (2.2 g cm^{-3}). Results for weak

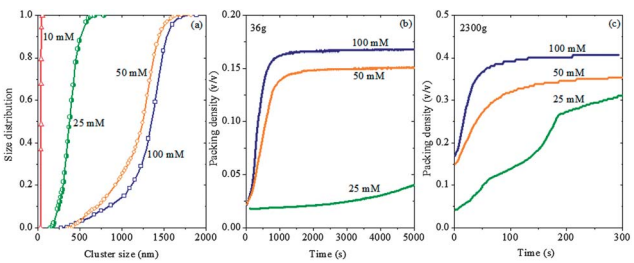

Fig. 2 Results of analytical centrifuge studies: (a) cumulative size distribution for silica–lysozyme aggregates at four different salinities indicating the increase in average aggregate size with the concentration of added NaCl; (b) and (c) packing density of the silica–lysozyme aggregates as a function of time at different salt concentrations from the sedimentation kinetics measured at 36g and 2300g, respectively.

Table 3 Size and size distribution of hetero-aggregates in system A ($y = 38$) at pH $\approx$ 11 at different salt concentrations[a]

c_{NaCl}/mM	L/nm	$\Delta L/L$
10	37	0.11
25	350	0.28
50	1056	0.27
100	1167	0.25

[a] c_{NaCl}, the concentration of the added NaCl; L, the mean size of aggregates; ΔL, the standard deviation of the size distribution.

and strong sedimentational compression (36*g* and 2300*g*) at three different salt concentrations at pH 11 are shown in Fig. 2b and c. For the lowest salt concentration (10 mM) no flocculation was detectable. The sample with 25 mM salt showed very slow sedimentation at 36*g*, and no sharp boundary between the sediment and the supernatant was observed after prolonged centrifugation. At higher salt concentrations the packing density quickly increased with time, reaching values $\varphi_s = 0.14$ and 0.16, respectively, at 50 mM and 100 mM salt concentrations (Fig. 2b). The faster sedimentation and larger silica volume fraction in the sediment attained at 100 mM salt concentration is a signature of larger and more compact aggregates. The samples were then subjected to a centrifugal stress of 2300*g*, leading to limiting volume fractions $\varphi_{s,max}$ of 0.34 and 0.40, respectively for 50 mM and 100 mM salt, while for 25 mM salt the limiting value of φ_s was not attained in the observation time (300 s). The error in φ_s resulting from the determination of V_{sed} for the 25 mM salt sample was higher than for the strongly aggregated dispersions (50 and 100 mM).

4.3 Structure factor and effective particle interaction

SAXS was used to characterize the effective interaction between silica particles induced by protein adsorption at different protein-to-silica particle number ratios *y*. A study covering the entire pH range from pI of silica to pI of the protein was made at $y = 38$ (sample A in Table 2). Complementary measurements in the complete-protein-binding regime at pH 8.3 were made for sample B ($y = 11$) and also samples with *y* up to 100.

Scattering profiles $I(q)$ for sample A at several pH values are shown in Fig. 3 for a low and a high salt concentration (10 and 100 mM). At high values of the scattering vector ($q > 0.5$ nm^{-1}; $Rq > 4.6$), all scattering curves are in agreement within experimental accuracy with $I(q)$ of the silica sample without the protein (Fig. 3a and c). This is expected because scattering is dominated by the silica particles (see Appendix). On the other hand, pronounced differences in $I(q)$ appear in the low-*q* region (Fig. 3b and d) as a function of pH at given ionic strength, and also for different ionic strengths at given pH. At pH < 4 and low ionic strength (10 mM) the scattering curves resemble that of bare silica. $I(q)$ approaches a constant limiting value at $q < 0.1$ nm^{-1}, indicating a stable colloidal dispersion. This is in line with the observation that no protein binds to the silica particles at low pH (Fig. 1a). At pH > 4, when the silica particles attain a surface charge opposite to that of the protein, scattering curves with steeply increasing low-*q* intensity are observed, This low-*q* scattering behavior conforms to a power-law $I(q) \propto q^{-n}$ and indicates formation of large-scale aggregates in the dispersion. Increasing the ionic strength also affects the low-*q* scattering behaviour, but its influence depends markedly on pH. A strong influence of ionic strength is found around pH 5 and an even stronger influence near pH 10, where silica–lysozyme aggregates re-disperse in the absence of salt, but form densely packed flocs at 50 and 100 mM salt (Fig. S3 in the ESI†). Salt-induced flocculation of the dispersion at pH 10 is demonstrated by the increasing value of the power-law exponent *n* of the low-*q* scattering regime, from $n \approx 1.5$ at 10 mM to $n > 3$ at 100 mM salt concentration. In the regime between pH 5 and 10, the influence of the added salt on the scattering curves is less pronounced. Table 4 summarizes the values of the power-law exponent *n* derived from the scattering curves for pH 5.0, 6.7, and 10 at different concentrations of the added salt.

The structure factor $S(q)$ was determined from the scattering curves of the silica–protein dispersions using eqn (2). Results for several salt concentrations at pH ≈ 5 and pH ≈ 10 are shown in Fig. 4a and b, respectively. The $S(q)$ data exhibit an oscillatory behavior. The primary maximum in $S(q)$ increases in amplitude with the increasing salt concentration, indicating a stronger effective interaction between the silica particles at higher ionic strength. This is in contrast to the behavior of the silica system without the protein, in which increasing ionic strength causes a damping of the oscillations in $S(q)$.[41] The scattering profiles in Fig. 4a and b also exhibit a weak secondary maximum, but the quality of the $S(q)$ data in that *q* region is blurred by the limited precision of the polydispersity of the bare silica nanoparticles, as explained elsewhere.[23] Another distinctive feature is the increase of $S(q)$ at $q < 0.2$ nm^{-1} which is pronounced at low ionic strength but not at high ionic strength (100 mM).

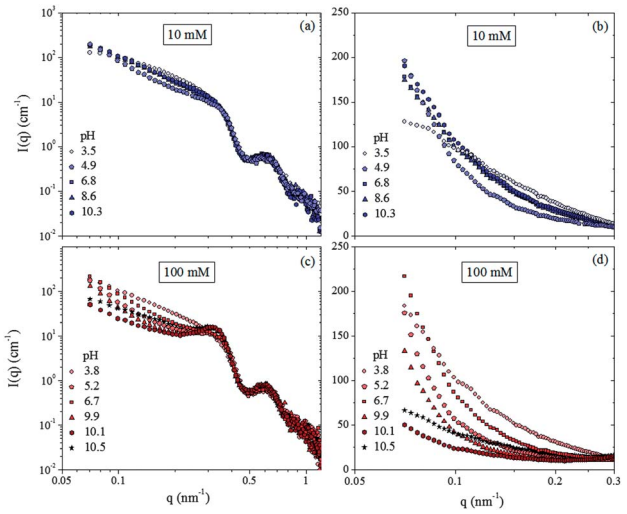

Fig. 3 SAXS intensity profiles $I(q)$ for the protein–silica sample A ($y = 38$) at different pH values, as indicated by the symbols and numbers in the graphs: (a) and (b): at 10 mM NaCl; (c) and (d) at 100 mM NaCl. The graphs in (a) and (c) show the complete $I(q)$ curves plotted on a log–log scale. Scattering profiles in (b) and (d) show the low-*q* region of the scattering curves at 10 and 100 mM, respectively, on a linear intensity scale.

Table 4 Parameters *n* ($I(q) \propto q^{-n}$) for sample A at different pH and salt concentrations

c_{NaCl}	*n* at pH 5.0	*n* at pH 6.7	*n* at pH 10
0	2.1	1.5	0.9
10	2.6	1.4	1.4
25	2.7	2.1	2.1
50	2.9	2.6	3.0
100	3.6	2.7	3.7

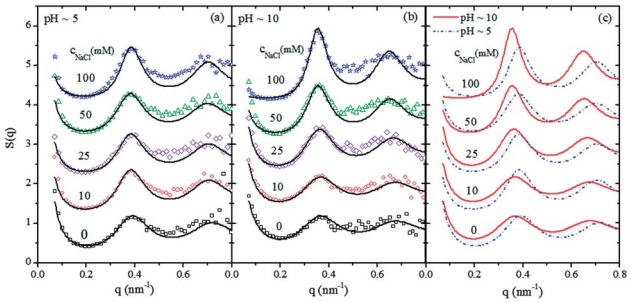

Fig. 4 Structure factor $S(q)$ derived from experimental scattering profiles $I(q)$ for protein–silica sample A ($y = 38$) at different salt concentrations c_{NaCl} as indicated in the figures: (a) at pH 5; (b) pH 10. Experimental data are shown by the symbols, the lines represent fits by the square-well potential; (c) comparison of the fit results for pH 5 and pH 10 at different electrolyte concentrations. The fit parameters for different pH and salt concentrations are shown in Fig. 5.

The $S(q)$ data were analyzed with the fluid model of particles interacting by a square-well potential, using the mean particle diameter D of Table 1 for the hard-core diameter of the pair potential ($\sigma = D$). Fits are shown by the full lines in Fig. 4a and b. The data are well reproduced in the q range below 0.4 nm^{-1}, where experimental artifacts are not playing a significant role. In particular, the position and height of the primary maximum and the behaviour at low q are well reproduced by this model. Similar fits were obtained for the data at other pH values. Fig. 5 shows values of the fit parameters Δ, ε and φ for the complete set of $S(q)$ data as a function of pH for different salt concentrations. The main results are as follows: the well width Δ increases with pH to values near 2 nm ($\Delta/\sigma \approx 0.1$) at pH 9, nearly independent of the salt concentration. At pH > 9 a steeper increase to values beyond 3 nm ($\Delta/\sigma \approx 0.15$) is observed at high salt concentrations. For the well depth ε values between 2 kT and 3 kT are found, decreasing with increasing pH, but with pronounced excursions to higher values near pH 5 and pH 10 at high salt concentrations. For the packing fraction φ a strong dependence on the ionic strength is found: at a low salt concentration (10 mM) it reaches a maximum value $\varphi \approx 0.15$ near pH 5 and falls off to low values at high pH. At a high salt concentration (100 mM) the maximum near pH 5 becomes much more prominent and a sharp increase to values $\varphi \approx 0.30$ occurs near pH 10. Except for the specific effects near pH 5 and pH 10, the graphs in Fig. 5a and b indicate opposite trends of the parameters ε and Δ as a function of pH. These antagonistic changes in the potential well parameters must be taken with reservation, because different combinations of Δ and ε can give fits of nearly the same quality. This situation is characteristic of systems interacting by a short-range potential, as in the present case where $\Delta/\sigma < 0.1$ (except at pH > 9). As explained in Section 2.2, the parameters ε and Δ can be replaced by the more robust stickiness parameter τ_e given by eqn (4). Values of τ_e^{-1} calculated by this relationship are shown in Fig. 5d. At low ionic strength τ_e^{-1} first increases with pH and then stays nearly constant at $\tau_e^{-1} \approx 11$ over a wide pH range. At higher ionic strength pronounced maxima in τ_e^{-1} appear near pH 5 and pH 10, reflecting the respective local maxima in the parameter ε of the square-well potential (Fig. 5b). We return to this salt influence on the effective stickiness in Section 5.2.

Sample B ($y = 11$; see Table 2) was studied at pH 8.3 at several salt concentrations up to 100 mM. Fig. 6 presents the SAXS profiles $I(q)$ and an analysis of the structure factor $S(q)$ on the

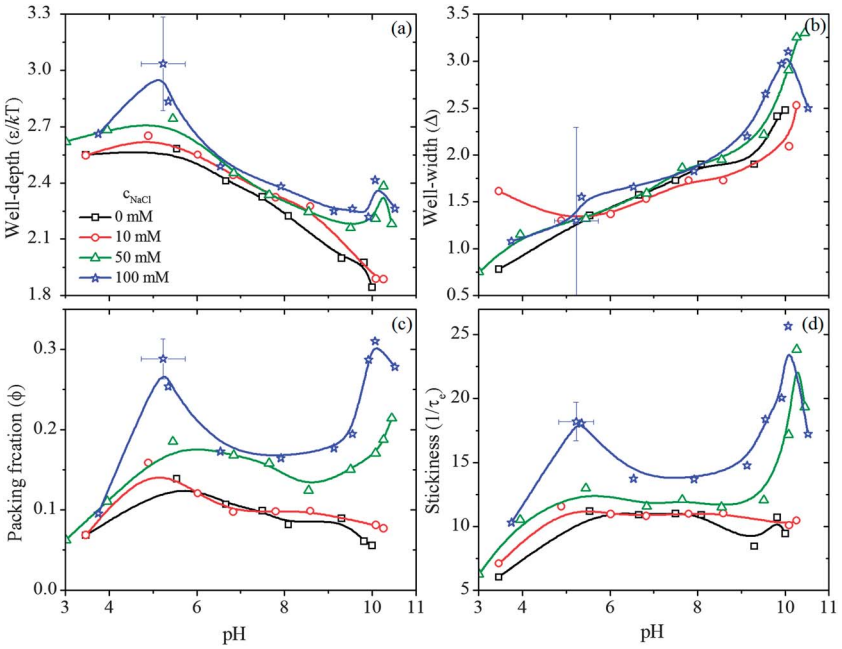

Fig. 5 Analysis of structure factor data in terms of the square-well fluid model for system A ($y = 38$). Values of the fit parameters (a) well-width Δ; (b) well depth ε/k_BT; (c) particle volume fraction in the aggregates φ, plotted as a function of pH for different salt concentrations from 0 to 100 mM. The graphs in (d) show the effective stickiness τ_e^{-1} as obtained from the parameters Δ and ε/k_BT by eqn (4).

basis of the square-well fluid model. Here again, all scattering curves are in agreement with that of the silica dispersion without the protein in the region of high scattering vector ($q > 0.45$ nm^{-1}; $Rq > 4.8$), and power-law behavior as $I(q) \propto q^{-n}$ is observed in the low-q region (at $q < 0.15$ nm^{-1}). Results of a quantitative analysis of the power-law region and of the structure factor in terms of the SWPY model are summarized in Table 5. The exponent n has a value close to zero at low ionic strength (up to 10 mM), but a high value at the highest 100 mM NaCl, indicating that large-scale aggregates are formed only at high ionic strength at pH 8.3. Analysis of the structure factor data with the SWPY model yields square-well potential parameters Δ and ε both increasing with the ionic strength. Since the pair potential is again short-ranged (relative well width $\Delta/\sigma < 0.08$ in all cases), the main information that can be extracted from $S(q)$ is the effective stickiness τ_e^{-1} and volume fraction φ of silica particles in the aggregates (Table 5). The pronounced increase in effective stickiness with the concentration of the added electrolyte in this system is shown in Fig. 6d. This behavior is remarkably different from the weak influence of ionic strength on the stickiness observed in system A at pH 8.3 (see Fig. 5d). To better understand this influence of the lysozyme-to-silica particle number ratio on the effective stickiness τ_e^{-1} of the silica particles, we performed SAXS measurements on samples with several different particle number ratios y at pH 8.3, and analyzed the structure factor $S(q)$ in the same way as explained above. Fig. 7 shows the resulting values of the effective stickiness τ_e^{-1} plotted as a function of the particle number ratio y. This graph clearly demonstrates that the number of protein molecules per silica particle strongly affects the aggregation behavior at low ionic strength and low y,

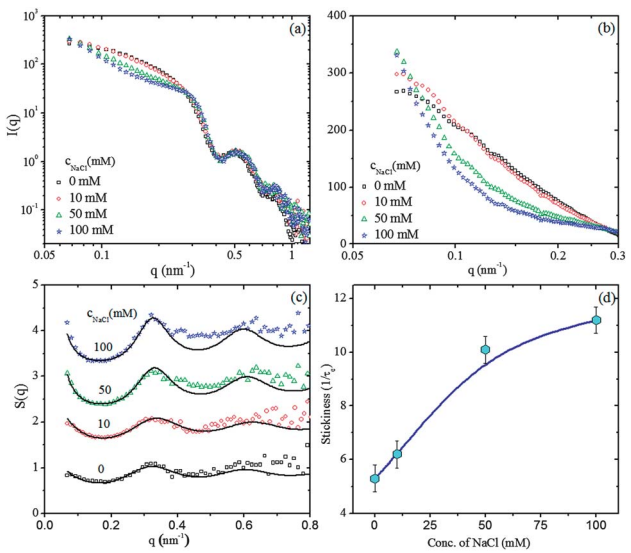

Fig. 6 SAXS scattering intensity profile $I(q)$ for lysozyme–silica system B ($y = 11$) at pH 8.3 and different salt concentrations: (a) complete $I(q)$ curves plotted on a log–log scale; (b) low-q region of the scattering curves plotted on a linear intensity scale; (c) experimental structure factor derived from $I(q)$ data and fits by the square-well potential; (d) resulting values of the effective stickiness τ_e^{-1} as a function of salt concentration at pH 8.3.

Table 5 Analysis of the structure factor data for System B ($y = 11$) at pH 8.3: slope n of the low-q region in $I(q)$, and parameters of the SWPY fluid model: well width Δ, well depth ε/kT, equivalent stickiness $1/\tau_e$, and effective volume fraction φ of particles in the aggregates[a]

c_{NaCl}	n	Δ/nm	ε/kT	$1/\tau_e$	φ
0	0.01	1.2	2.1	5.3	0.08
10	0.03	1.5	2.1	6.2	0.09
50	1.9	1.3	2.7	10.1	0.16
100	2.5	1.7	2.5	11.2	0.15

[a] All measurements were made at 25 °C.

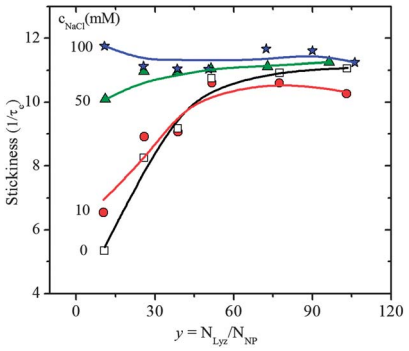

Fig. 7 Effective stickiness τ_e^{-1} of the silica particles as a function of the protein-to-silica particle number ratio y in the complete-protein-binding regime (pH = 8.3) for different salt concentrations (0, 10, 50 and 100 mM).

where the effective particle stickiness sharply decreases with decreasing y, but not at high ionic strength and high y where the particle stickiness becomes nearly independent of the number of protein molecules per silica particle.

5. Discussion

5.1 Protein binding

The present results support earlier reports[7–11,42–44] that the adsorption of lysozyme on silica surfaces is mainly due to electrostatic interactions. This is concluded from the fact that the sharply increasing protein binding curve (Fig. 1a) correlates with the pH dependence of the charge density of silica surfaces.[45] According to the potentiometric titration of a nanoscale pure silica surface[46] the negative surface charge density increases from a very low value ($< 3 \times 10^{-4}$ e$^-$ per nm^2) at pH 5 to *ca.* 0.015 e$^-$ per nm^2 at pH 7 and 0.035 e$^-$ per nm^2 at pH 8 (values read from Fig. 2 of ref. 46). A similar value (0.016 e$^-$ per nm^2 in pure water at pH 6) was reported by Zeng *et al.*,[29] while somewhat higher values (0.09 and 0.15 e$^-$ per nm^2, respectively, for pH 6 and 7 in 1 mM NaCl) were given by Shin *et al.*[47] Due to the low charge density of the silica surface at low pH the mean distance between two charged surface sites exceeds the footprint length of a lysozyme molecule. This implies that the individual protein molecules can bind to only a single charged surface site. Nevertheless, adsorption isotherms in the pH 5–7 regime exhibit a high-affinity character like those at higher

pH.[23] This indicates that binding to a single charged surface site is sufficient for high-affinity adsorption of lysozyme on the silica surface. Specifically, for our sample A (0.64 mg lysozyme per m^2, corresponding to a surface concentration Γ_0 of 0.027 molecules per nm^2; see Table 2) the surface charge densities of silica reported in ref. 46 suggest that complete protein binding ($f = 1$) should be reached at a pH somewhat above pH 7, in agreement with the experimental finding (Fig. 1a). Note that the limiting surface concentration of $\Gamma_0 = 0.027$ nm^{-2} for sample A corresponds to only one third of the maximum monolayer adsorption ($\Gamma_0 = 0.083$ nm^{-2}) estimated from the footprint area of lysozyme molecules adsorbed side-on (*ca.* 12 nm^2). For the partial binding regime ($f < 1$), *i.e.*, when protein binding is limited by the available surface charge, our results then indicate that the adsorbed lysozyme molecules bind to single ionized surface groups. This case resembles the scenario reported by Shin *et al.*[48] for the adsorption of polyelectrolyte oligomers on silica in a similar pH regime. In the present work, a complete monolayer of protein ($\Gamma_0 = 0.083$ nm^{-2}) is attained only by the sample with the highest protein-to-silica particle number ratio ($y = 100$) at pH 8.3, while for sample A nearly 65% of the surface remains free from the protein (more than 90% for sample B) in the complete-protein-binding regime.

The insensitivity of the protein binding curve against the added electrolyte in the charge limited regime below pH 8 (Fig. 1a) is surprising in view of earlier studies[4,6,8,9,42,43] which reported that increasing ionic strength is causing a decrease in adsorption of lysozyme on silica surfaces. Tentatively, we attribute the observed insensitivity of the binding characteristics against salt to a compensation of two opposing effects: (a) increasing silanol dissociation due to the added salt;[45,46,49] (b) counter-ions of the salt competing with the protein for the charged surface sites. According to Shin *et al.*,[48] binding of sodium counter ions to charged silanol groups plays no significant role in the relevant pH regime (less than 1% of the negative surface sites up to pH 8). Preliminary results of a systematic study of the salt effect on the adsorption isotherms[50] indicate that the insensitivity against the salt concentration is limited to the charge-limited regime below pH 8, while at higher pH the expected decrease in adsorption with increasing ionic strength is observed. Hence, our results do not contradict reports on salt effects on the adsorption at pH > 8, as in the work of Lundin *et al.*[43]

5.2 Bridging aggregation

Aggregation and flocculation in our system is attributed to bridging of silica particles by lysozyme molecules. In order to act as a bridge the protein must have binding sites on opposite sides of the molecule. Surface patches having a high positive electrostatic potential will represent strong binding sites for the negative surface of the silica particles. Electrostatic potential calculations[51] for patches of the lysozyme surface (0.5 nm radius) showed that the N-terminal amino acid lys 1 represents the most positive patch, followed by lys 13 and lys 116. While lys 13 is situated not far apart from lys 1, lys 116 is nearly on the opposite side of the molecule and may thus represent a binding site for the second silica particle in the bridging geometry. Equivalent conclusions resulted from an experimental search for favourable binding orientations of lysozyme on negatively charged surfaces, which also indicated that pH may have a pronounced influence.[51] Obviously, from the present results we cannot decide which of the basic amino acids forms the binding site on the lysozyme molecule.

The present work shows that the ionic strength is strongly affecting the bridging aggregation, although no influence on protein binding to the silica particles is detectable (Fig. 1). The influence of the added salt on the hetero-aggregation is demonstrated by the increase in aggregate size and packing density found in the centrifugation study (Fig. 2), and by the low-q scattering behaviour of the SAXS intensity profiles (Fig. 3b and d). The increase in the primary maximum of $S(q)$ (Fig. 4 and 6c) also indicates an increase in the particle packing density in the hetero-aggregates when the salt concentration is increased. Moreover, we find that the influence of ionic strength on the bridging interaction of the protein with the silica particles varies with pH. The effective stickiness τ_e^{-1} of the silica particles in the silica–protein dispersions can be used to characterize the strength of the bridging interaction. As shown in Fig. 5d, an increase in salt concentration from 10 to 100 mM causes a pronounced increase in τ_e^{-1} in pH ranges near pH 5 and 10, but it shows only a moderate increase in the intermediate range from pH 6 to 9.

The marked salt effect at pH 5 may be rationalized by remembering that in the low protein binding regime, the low surface charge of the silica particles limits the number of highly charged protein molecules that are bound. Screening of the repulsive interaction may then favour bridging configurations in which silica particles come into close contact with their next neighbours, while the bridging protein molecule occupies binding sites close to the particle–particle contact point. In such a configuration the van der Waals interaction will contribute to the attractive interaction between the silica particles and to their effective stickiness. As pH is raised and more protein molecules are bound to the silica particles, low-coordinated open aggregate structures will be favoured to reduce the repulsive electrostatic interaction between protein molecules adsorbed on neighbouring particles. The added electrolyte causes a decrease of the effective charge on the lysozyme molecules,[52–54] and thus weaker repulsive interactions between protein molecules adsorbed near the bridging contact of neighbouring particles. The lower repulsive strain resulting from screening the repulsive interaction between adsorbed protein molecules can possibly explain the somewhat higher effective stickiness of the silica particles at higher ionic strength observed in this intermediate pH regime from pH 6 to 9 (Fig. 5d).

Above pH 9 the net positive charge of lysozyme molecules decreases sharply as the isoelectric point is approached, but some of the positive binding sites persist up to pH > pI.[51] The electrostatic repulsion between the highly charged silica particles opposes the bridging by the protein and eventually causes the breaking of silica–protein bonds and re-dispersion of the silica at pH > 9. In the presence of the electrolyte, this repulsive interaction between the silica particles is screened and bridging of silica particles by protein molecules can sustain. Close to pI of

the protein, attractive interactions between adsorbed, but non-bridging protein molecules may also add to the stability of the hetero-aggregates. Specifically, the release of bound Cl^- counter ions and partial dehydration of the surface that would expose hydrophobic patches of the protein surface to the solution may cause hydrophobic aggregation of lysozyme similar to the case of crystallization–precipitation at pH 10–11 and high salt concentration.[52] Indeed, hydrophobic interactions between adsorbed protein molecules may be the driving force of hetero-aggregation in this regime. This effect becomes stronger with increasing salt concentration and may cause the observed increase in the mean aggregate size and the packing density of the flocs (Fig. 2).

5.3 Influence of the protein concentration

The strength of the bridging interaction and its dependence on the ionic strength are affected by the protein-to-silica number ratio $y = N_{Lyz}/N_{NP}$. This influence exists in the complete-protein-binding regime at high pH, but not at lower pH, where protein binding is limited by the low charge density of the silica surface (see Section 5.1). The influence of ionic strength on the bridging interaction is most pronounced at low y. This trend is brought out clearly by the dependence of the effective stickiness parameter τ_e^{-1} on the particle number ratio y in Fig. 7. At the lowest protein-to-silica particle number ratio studied in this work ($y = 11$), weak hetero-aggregation in the absence of salt is indicated by a low effective stickiness τ_e^{-1}, but pronounced hetero-aggregation occurs at 100 mM salt concentration, indicated by the high value of the effective stickiness (Fig. 6). This strong influence of ionic strength on the effective stickiness at low protein concentrations reflects the competition between attractive protein bridging and repulsive electrostatic interaction between the highly charged silica particles in the aggregates. At low ionic strength the repulsive interaction between the particles dominates, but this repulsive interaction is screened at higher ionic strength. At higher concentration of the protein on the silica particles (higher y) the high surface charge of the silica particles is partly shielded by the opposite charge of the adsorbed lysozyme, so that the bridging interactions dominate even at low salt concentrations. Hence the trends shown in Fig. 7 reflect the complex interplay between the surface-specific protein binding and bridging interactions and the unspecific electrostatic interactions between the charged silica and protein particles as a function of pH and ionic strength. We remark that the strong influence of ionic strength manifested at low protein-to-silica particle number ratio y in the complete-protein binding regime at pH 8.3 (Fig. 6d) has a different origin from the somewhat similar effects seen in the low protein binding regime at pH 5 (Fig. 5d). As explained in Section 5.2, we propose that in this case screening of the weak electrostatic interaction between the silica particles allows for close contacts between the particles, so that attractive van der Waals interactions will add to the protein bridging interaction and cause a high effective stickiness of the particles.

5.4 Phase behaviour

In Section 4.3 it was shown that the effective interaction between silica particles in the bridging aggregates can be represented by the SHS model. The phase diagram of the SHS fluid contains a liquid/vapour coexistence region with the critical point located at a reduced critical temperature $\tau_c = 0.113$ ($\tau_c^{-1} = 8.8$) and critical density $n_c\sigma^3 = 0.508$ ($\varphi_c = n_c\sigma^3\pi/6 = 0.266$).[55] For colloidal dispersions the two-phase region corresponds to a flocculation into large-scale aggregates in coexistence with monomers and small aggregates. The SHS model also predicts percolation, and the vapour–liquid critical point lies at a density far beyond the percolation threshold.[55,56] This implies that the flocculate phase will consist of fully percolated aggregates, consistent with our picture of large-scale bridging aggregates. Since the effective interaction among silica particles in these aggregates depends on pH and ionic strength, data obtained at a constant temperature but at different values of pH and/or ionic strength correspond to different reduced temperatures τ_e in the phase diagram. When expressed by the stickiness τ_e^{-1}, values less than the critical value $(\tau_e^{-1})_c = 8.8$ correspond to states in the one-phase region and values greater than 8.8 correspond to states in the two-phase region. The results of our study are consistent with this prediction. As shown in Fig. 5d, we find low values of the stickiness ($\tau_e^{-1} < 8.8$) at pH < 4, where no flocculation occurs, but high values ($\tau_e^{-1} > 10$) in the pH range of 4 to 9, in which large-scale flocculation is observed. Near pH 10, very high values of τ_e^{-1} are found at high ionic strength (100 mM), but values well below the critical value 8.8 are found at low ionic strength, consistent with the fact that re-dispersion of the flocculate occurs above pH 10 in the absence of the added salt (as documented in Table 4 of our earlier paper[23]).

We interpret the parameter φ extracted from the structure factor $S(q)$ as a measure of the packing fraction of silica particles in the aggregates. Qualitatively, the trends in the values of φ as a function of pH and ionic strength are similar to those for the stickiness τ_e^{-1} (Fig. 5c and d); relatively low values ($\varphi = 0.05$ or less) are found for samples in the one-phase region of the phase diagram ($\tau_e^{-1} < 8.8$), but values up to $\varphi = 0.30$ are found for samples in the two-phase region ($\tau_e^{-1} > 8.8$). For the two-phase region this trend is expected from the shape of the coexistence curve, as the density of the condensed phase increases with decreasing temperature. Accordingly, the high values of φ at pH 5 and 10 at high salt concentrations can be traced back to the strong bridging interaction (high effective stickiness τ_e^{-1}), which implies a low reduced temperature τ_e in the phase diagram. Hence the qualitative behaviour of our system can be rationalized on the basis of the one-component SHS model. However, the values of φ extracted from the structure factor are lower than expected from the phase diagram of the SHS model obtained by Grand Canonical Monte Carlo simulations.[55] For example, the value obtained for the lowest temperature ($\varphi \approx 0.30$ at $\tau_e^{-1} \approx 25$) is not much higher than the critical density obtained in the GCMC simulations ($\varphi_c \approx 0.27$), although this density corresponds to a very low reduced temperature ($\tau_e/\tau_{e,c} \approx 0.35$). The values of φ extracted from the structure factor data for pH 10 (Fig. 5c) are also somewhat lower than the packing densities of the flocculate derived from the centrifugation study (Fig. 2c). Such deviations are not unexpected in view of the simplicity of the underlying model.

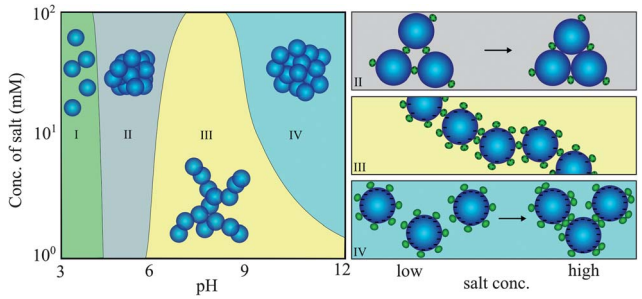

Fig. 8 Different regions of protein binding and bridging aggregation of lysozyme with silica nanoparticles as a function of pH and salt concentration.

Table 6 Estimation of the scattering contributions of each component towards the total intensity for silica and lysozyme dispersion in water[a]

Material	R_g (nm)	ρ_m g cm^{-3}	ρ_{SLD} ($\times 10^{10}$) cm^{-2}	$\Delta\rho_{SLD}{}^2 \times R_g{}^3$ cm^{-1}
H_2O	—	0.99	9.4	—
Lysoyzme	1.5	1.35	12.3	2.8
Silica	10.8	2.25	19.2	12.3×10^3

[a] R_g is the radius of gyration, ρ_m is the mass density in g cm^{-3}, ρ_{SLD} is the Cu-K$_\alpha$ scattering length density in cm^{-2}, and $\Delta\rho_{SLD}$ is the scattering contrast in water (ρ_{SLD}–$\rho_{SLD}(H_2O)$).

6. Conclusions

We have studied the combined influence of pH and ionic strength on the binding of lysozyme to silica nanoparticles and the protein-induced aggregation of the particles. Our results support the notion that lysozyme molecules can bind to negative surface sites by ion pair formation with one of the strongly charged lys (or arg) residues of the protein, and that up to pH 7 the protein adsorption is limited by the number of charged surface groups. For this pH regime it is found that the protein binding curve is essentially unaffected by the ionic strength.

The effective interaction between silica particles caused by protein bridging was extracted from the SAXS structure factor data with a structure factor model based on a square-well pair potential close to the sticky-hard-sphere limit. The effective stickiness τ_e^{-1} and packing fraction φ of the particles represent useful parameters to characterize the bridging aggregates as a function of pH and ionic strength. A pronounced increase of τ_e^{-1} and φ with the ionic strength is found near pH 5 and pH 10, but we argue that the high stickiness and packing fraction of the particles in these two pH regions have a different origin.

In Fig. 8 the combined influence of the salt concentration and pH on the hetero-aggregation is sketched by regions I–IV. At low pH (region I) the silica particles are nearly uncharged and lysozyme is not adsorbed. Weak aggregation of the silica particles resulting from absent charge stabilization in this regime is indicated by a low effective stickiness. In the partial-protein-binding regime at higher pH (region II), bridging of silica particles by a small number of protein molecules can lead to aggregates of fairly high packing density. In this regime, screening of the weak repulsive electrostatic interaction between the silica particles can cause the particles to approach each other more closely without loss of the bridging interaction by the protein molecules. In the complete-protein-binding regime above pH 6 (region III), repulsive interactions between the protein molecules adsorbed at close distances on neighbouring silica particles are favouring low-coordinated open aggregates. As the repulsive interaction among these protein molecules is screened by the added salt, the effective particle interaction and the packing density increase. Screening of the repulsive electrostatic interactions between the highly charged silica particles is the dominating salt effect in region IV. In the proximity of the isoelectric point of lysozyme (pI $\approx$ 10.7) hydrophobic interactions between adsorbed protein molecules also add to the high effective stickiness found at high salt concentrations in this regime.

Hence the present results show that pH and ionic strength determine the bridging aggregation behaviour in this system, in spite of the fact that protein binding to the silica particles is almost unaffected by the ionic strength at the protein concentrations chosen in this study. Another important finding of this work is that the protein–silica hetero-aggregates can be analysed on the basis of effective interactions of a single-component square-well fluid. Further work is needed to assess the scope of applicability of this approach.

Appendix

Table 6 gives an estimate of the scattering contributions of the silica particles and lysozyme to the overall scattering. According to this estimate the scattering contribution of the protein is smaller than that of the silica particles by nearly a factor of 4000.

Acknowledgements

We wish to thank M. Ballauff, R. von Klitzing, D. Lerche, M. Schoen and O. D. Velev for helpful discussions on different aspects of this work. Financial support by the Deutsche Forschungsgemeinschaft (DFG) in the framework of IRTG 1524 is gratefully acknowledged.

Notes and references

1 M. E. Aubin-Tam and K. Hamad-Schifferli, *Biomed. Mater.*, 2008, **3**, 034001.
2 M. Mahmoudi, I. Lynch, M. R. Ejtehadi, M. P. Monopoli, F. B. Bombelli and S. Laurent, *Chem. Rev.*, 2011, **111**, 5610–5637.
3 A. S. Shematov, I. Nabiev and A. Sukhanova, *ACS Nano*, 2012, **6**, 4585–4602.
4 C. M. Roth and A. M. Lenhoff, *Langmuir*, 1995, **11**, 3500–3509.
5 M. Wahlgren, T. Arnebrant and I. Lundström, *J. Colloid Interface Sci.*, 1995, **175**, 506–514.
6 J. Buijs and V. Hlady, *J. Colloid Interface Sci.*, 1997, **190**, 171–181.

7 H. Larsericsdotter, S. Oscarsson and J. Buijs, *J. Colloid Interface Sci.*, 2001, **237**, 98–103.
8 M. van der Veen, W. Norde and M. Cohen Stuart, *Colloids Surf., B*, 2004, **35**, 33–40.
9 P. M. Biesheuvel, M. van der Veen and W. Norde, *J. Phys. Chem. B*, 2005, **109**, 4172–4180.
10 R. A. Hartvig, M. van de Weert, J. Østergaard, L. Jorgensen and H. Jensen, *Langmuir*, 2011, **27**, 2634–2643.
11 F. Felsovalyi, P. Mangiagalli, C. Bureau, S. K. Kumar and S. Banta, *Langmuir*, 2011, **27**, 11873–11882.
12 W. Norde, in *Biopolymers at Interfaces*, ed. M. Malmsten, Marcel Dekker, New York, Basel, 2nd edn, 2003.
13 W. Norde, *Colloids Surf., B*, 2008, **61**, 1–9.
14 A. A. Vertegel, R. W. Siegel and J. S. Dordick, *Langmuir*, 2004, **20**, 6800–6807.
15 M. Lundquist, I. Sethson and B.-H. Jonsson, *Langmuir*, 2004, **20**, 10639–10647.
16 P. Roach, D. Farrar and C. C. Perry, *J. Am. Chem. Soc.*, 2006, **128**, 3939–3945.
17 W. Shang, J. H. Nuffer, V. A. Muniz-Papandrea, W. Colón, R. W. Siegel and J. S. Dordick, *Small*, 2009, **5**, 470–476.
18 X. Wu and G. Narsimhan, *Biochim. Biophys. Acta*, 2008, **1784**, 1694–1701.
19 G. Anand, S. Sharma, A. K. Dutta, S. K. Kumar and G. Belfort, *Langmuir*, 2010, **26**, 10803–10811.
20 S. Linse, C. Cabaleiro-Lago, W.-F. Xue, I. Lynch, S. Lindman, E. Thulin, S. E. Radford and K. A. Dawson, *Proc. Natl. Acad. Sci. U. S. A.*, 2007, **104**, 8691–8696.
21 S. Goy-López, J. Juárez, M. Alatorre-Meda, E. Casals, V. F. Puntes, P. Taboada and V. Mosquera, *Langmuir*, 2012, **28**, 9113–9126.
22 S. Kumar, V. K. Aswal and J. Kohlbrecher, *Langmuir*, 2011, **27**, 10167–10173.
23 B. Bharti, J. Meissner and G. H. Findenegg, *Langmuir*, 2011, **27**, 9823–9833.
24 B. Bharti and G. H. Findenegg, *Chem. Lett.*, 2012, **41**, 1122–1124.
25 A. E. Nel, L. Mädler, D. Velegos, T. Xia, E. M. V. Hoek, P. Somasundaran, F. Klaessig, V. Castranova and M. Thompson, *Nat. Mater.*, 2009, **8**, 543–557.
26 C. C. F. Blake, D. F. Koenig, G. A. Mair, A. C. T. North, D. C. Phillips and V. R. Sarma, *Nature*, 1965, **206**, 757–761.
27 L. Shi, F. Carn, F. Boué, G. Mosser and E. Buhler, *Soft Matter*, 2013, **9**, 5004–5015.
28 D. Qiu, T. Cosgrove, A. M. Howe and C. A. Dreiss, *Langmuir*, 2006, **222**, 546–552.
29 Y. Zeng, S. Grandner, C. L. P. Oliveira, A. F. Thünemann, O. Paris, J. S. Pedersen, S. H. L. Klapp and R. von Klitzing, *Soft Matter*, 2011, **7**, 10899–10909.
30 A. Malijevsky, S. B. Yuste and A. Santos, *J. Chem. Phys.*, 2006, **125**, 074507.
31 R. J. Baxter, *J. Chem. Phys.*, 1968, **49**, 2770–2774.
32 D. Gazzillo and A. Giacometti, *J. Chem. Phys.*, 2004, **120**, 4742.
33 C. Regnaut and J. C. Ravey, *J. Chem. Phys.*, 1989, **91**, 1211–1221; C. Regnaut and J. C. Ravey, *J. Chem. Phys.*, 1990, **92**, 3250.
34 P. V. Sharma and K. C. Sharma, *Physica A*, 1977, **89**, 213–218.
35 C. G. de Kruif and J. A. Schouten, *J. Chem. Phys.*, 1990, **92**, 6098–6103.
36 T. M. Davis, M. A. Snyder, J. E. Krohn and M. Tsapatsis, *Chem. Mater.*, 2006, **18**, 5814–5816.
37 D. I. Svergun, S. Richard, M. H. J. Koch, Z. Sayers, S. Kuprin and G. Zaccai, *Proc. Natl. Acad. Sci. U. S. A.*, 1998, **95**, 2267–2272.
38 http://kur.web.psi.ch/sans1/SANSSoft/sasfit.html.
39 D. Lerche and T. Sobisch, *Powder Technol.*, 2007, **174**, 46–49.
40 T. Sobisch and D. Lerche, *Colloids Surf., A*, 2008, **331**, 114–118.
41 S. H. L. Klapp, D. Qu and R. V. Klitzing, *J. Phys. Chem. B*, 2007, **111**, 1296–1303.
42 T. Nezu, T. Masuyama, K. Sasaki, S. Saitoh, M. Taira and Y. Araki, *Dent. Mater. J.*, 2008, **27**, 573–580.
43 M. Lundin, U. M. Elofsson, E. Blomberg and M. W. Rutland, *Colloids Surf., B*, 2010, **77**, 1–11.
44 K. Kubiak-Ossowska and P. A. Mulheran, *Langmuir*, 2010, **26**, 7690–7694.
45 S. H. Behrens and D. G. Grier, *J. Chem. Phys.*, 2001, **115**, 6716–6721.
46 A. Salis, D. F. Parsons, M. Boström, L. Medda, B. Barse, B. W. Ninham and M. Monduzzi, *Langmuir*, 2010, **26**, 2484–2490.
47 Y. Shin, J. E. Roberts and M. Santore, *J. Colloid Interface Sci.*, 2001, **244**, 190–199.
48 Y. Shin, J. E. Roberts and M. Santore, *J. Colloid Interface Sci.*, 2002, **247**, 220–230.
49 B. Popping, B. Sebille, A. Deratani, N. Desbois, J. M. Lamarche and A. Foissy, *Colloids Surf.*, 1992, **64**, 125–133.
50 J. Meissner, B. Bharti and G. H. Findenegg, unpublished results.
51 F. Dismer, M. Petzold and J. Hubbuch, *J. Chromatogr., A*, 2008, **1194**, 11–21.
52 O. D. Velev, E. W. Kaler and A. M. Lenhoff, *Biophys. J.*, 1998, **75**, 2682–2697.
53 A. S. Parmer and M. Muschol, *Biophys. J.*, 2009, **97**, 590–598.
54 Y. R. Gokarn, R. M. Fesinmeyer, A. Saluja, V. Razinkov, S. F. Chase, T. M. Laue and D. N. Brems, *Protein Sci.*, 2011, **20**, 580–587.
55 M. A. Miller and D. Frenkel, *Phys. Rev. Lett.*, 2003, **90**, 135702.
56 H. Neitschand and S. H. L. Klapp, *J. Chem. Phys.*, 2013, **138**, 064904.

